Meltdown! Local Heating by Decaying Excited Host Positive Polarons Triggers Aggregation Quenching in Blue PhOLEDs**

Tobias Setzer,*[a] Pascal Friederich,[b] Velimir Meded,[b] Wolfgang Wenzel,[b] Christian Lennartz,[c] and Andreas Dreuw*[a]

Exciton-polaron induced aggregation (EPIA) in organic host materials for blue Phosphorescent Organic Light Emitting Diodes (PhOLEDs) is driven by a non-radiative decay of electronically excited positive polarons resulting in a local heating of the amourphous host matrix. The released heat triggers morphological changes, i.e. molecular aggregation between neighboring host molecules. The resulting aggregates, which our calculations identify as carbazolyl dimers, lead to decreased PhOLED efficiency. Statistical assessment of some host-only morphologies reveals a structure-dependent propensity for molecular aggregation corroborating the identified EPIA mechanism. Our findings provide a fresh look at established molecular design rules and will help to improve blue PhOLED host materials to enhance blue PhOLED device lifetimes.

1. Introduction

Driven by the rapid development of new displays for mobile devices, for instance smartphones and tablet computers, OLEDs (*Organic Light Emitting Diodes*) have started to surpass the established LCD (*Liquid Crystal Display*) technology in recent years.[1] Especially in phosphorescent OLEDs (PhOLEDs),which make use of spin-orbit coupling in late transition metals, like platinum and iridium, the internal quantum efficiency reaches 100 %.[2–4] These days, state-of-the-art red and green PhOLEDs are commercially available and widely used in the OLED display industry.[5] Yet, their blue equivalents are still subject of ongoing research as they suffer from severe long-term stability issues.[5–7]

While extrinsic degradation, like dark spot formation, electrical shortcuts or a sudden decrease in luminance, are technically solved by purification and encapsulation methods, intrinsic degradation processes still require additional fundamental research.[7,8] Recent findings on wide-band-gap host materials for blue PhOLEDs indicate, that exciton-polaron induced aggregation (EPIA) in the vicinity of interfaces isone of the major processes, that significantly reduces the OLED lifetime.[9–12] EPIA describes the aggregation of OLEDs induced by the interaction between an excited electronic state, the exciton, of an emitter molecule and aradical cation (positive polaron) or radical anion (negative polaron) of the host material. In other words, EPIA describes the interaction of an excited electronic singlet state with a radical exhibiting a doublet electronic state.

EPIA has been demonstrated to yield molecular aggregates, which have a narrower band-gap energy E_g and thus reduce the overall PhOLED efficiency.[9] These findings are corroborated by spectroscopic studies on the formation of carbazolyl triplet excimers in some CBP[1] derivatives.[13] In particular, it has recently been shown experimentally that exciton-induced morphological aggregation of carbazol based host materials is behind the appearance of long-wavelength bands and that complexation between the aggregated molecules and ETL molecules plays a role in this phenomenon. Comparisons between the effects of exciton and thermal stress suggest that exciton-induced aggregation may be limited to short-range molecular ordering or pairing (e.g., dimer or trimer species formation) versus longer-range ordering (crystallization) in the case of thermal stress.[12]

In this communication, the mechanism of this observed exciton-induced local aggregation is identified and the main source of EPIA is attributed to local heating by excited carbazolyl cations, so-called positive polarons, fully supporting the previous experiments. For that objective, we study carbazole based aggregates formed during EPIA by means of quantum chemical calculations and show a material-specific tendency of blue PhOLED host materials to form molecular aggregates during the deposition process. mCP[2], CBP and PCDC[3] (Figure 1) have beenused as representative host materials. Their photophysics, potential energy transfer channels and

[a] *Dr. T. Setzer, Prof. Dr. A. Dreuw*
Interdisziplinäres Zentrum für Wissenschaftliches Rechnen, Ruprecht Karls Universität Heidelberg, Im Neuenheimer Feld 205A, 69120 Heidelberg, Germany
E mail: tobias.setzer@iwr.uni heidelberg.de
dreuw@uni heidelberg.de
[b] *Dr. P. Friederich, Dr. V. Meded, Prof. Dr. W. Wenzel*
Institute of Nanotechnology, Karlsruhe Institute of Technology (KIT), Her mann von Helmholtz Platz 1, 76344 Eggenstein Leopoldshafen, Germany
[c] *Dr. C. Lennartz*
trinamiX GmbH, Industriestraße 35, 67063 Ludwigshafen am Rhein, Germany
[**] *PhOELEDs: Phosphorescent organic light emitting diodes*

[1] 4,4′ di(9*H* carbazol 9 yl) 1,1′ biphenyl

[2] 1,3 di(9*H* carbazol 9 yl)benzene

[3] 9 (3 (8 (9*H* carbazol 9 yl)dibenzo[*b*,*d*]furan 2 yl)phenyl) 9*H* carbazole

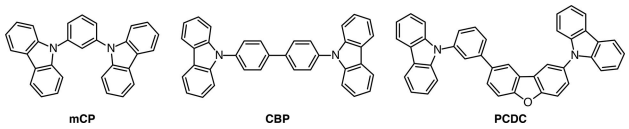

Figure 1. Molecular structures of the contemporary state of the art PhOLED host materials mCP[2], CBP[1] and PCDC[3].

the key mechanistic key features behind EPIA have also been investigated. In combination with the experimental findings,[12] new insights into the details of the degradation mechanism of blue PhOLEDs is gained to establish new molecular design principles to systematically improve the device lifetime of blue PhOLEDs.

2. Results and Discussion

In Figure 2 simulated fluorescence ($\Delta E(S_1)@S_1$)[4] and phosphorescence ($\Delta E(T_1)@T_1$)[4] emission energies of 9H-carbazole and its C_{2v} and C_{2h} symmetric dimers are shown. Methodological details as well as vertical and adiabatic excitation energies for the 9H-carbazole monomer and its two dimers can be found in Table S1 of the ESI. The computed 9*H*-carbazole fluorescence energy (3.92 eV) is 0.16 eV higher than the experimental absorption measurement in solution (3.76 eV[14,15]). Thus, our computations slightly overestimate the fluorescence energy, yet, the calculated gas-phase 9*H*-carbazole phosphorescence (3.12 eV) is in reasonable agreement with the experimental phosphorescence value measured in solution (3.04 eV[14,15]). Since the deviation from the experimental values is small, the ADC(2)/def2-SV(P) results are accurate enough to study general trends of the excited states and optical properties of 9*H*-carbazole and its dimers. For both, the C_{2v} and C_{2h} dimer, the computed fluorescence (2.95 eV for C_{2v} and 3.33 eV for C_{2h}) and phosphorescence energies (2.62 eV for C_{2v} and C_{2h}) are bathochromically shifted with respect to the monomer values. However, even when the systematic overestimation of the computed fluorescence values is taken into account, the simulated fluorescence energies $\Delta E(S_1)@S_1$ of the dimers neither explain the bathochromic shifts observed in electroluminescence spectra of degraded single-charge-carrier host-only devices[9] nor the excimer bands in thin films of some CBP derivatives.[13] In both cases the respective bathochromically shifted bands were observed at $\leq$2.5 eV.[9,13] On the other hand, the computed phosphorescence energies, $\Delta E(T_1)@T_1$, of both dimers are in very good agreement with the spectroscopic studies,in which formation of triplet excimers in some CBP derivatives has been suggested.[13] Thus, referring to existing literature, *bis*-carbazolyl host materials are prone to form molecular aggregates between the terminal carbazolyl groups of neighboring matrix molecules, which according to our calculations form triplet quenching states, that directly relate to a decreased PhOLED device efficiency.[12]

[4]vertical S_1 (T_1) excitation energy at the corresponding S_1 (T_1) optimized geometry

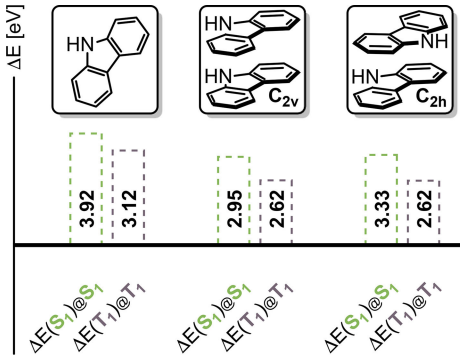

Figure 2. Simulated fluorescence ($\Delta E(S_1)@S_1$) and phosphorescence ($\Delta E(T_1)@T_1$) emission energies at the respective S_1 and T_1 geometries of the 9*H* carbazole monomer and its dimers in C_{2v} and C_{2h} symmetry. Excited state geometries and energies are obtained at the ADC(2)/def2 SV(P) level of theory.

To quantify the material-specific propensity of mCP, CBP and PCDC to form aggregates, simulated host-only morphologies were used to assess the number of readily formed carbazolyl dimer species in host-only morphologies (for computational details see section 5).

The heatmap representation in Figure 3a)–c) collects the number of nearest-neighbor carbazolyl-dimer pairs as a function of dimer stacking angle i and center-of-geometry distance d_{COG} between neighboring carbazolyl units. For $\phi = 0^\circ$ and $\phi = 180^\circ$, a (π-stacked) carbazolyl dimer is obtained, while for $\phi = 90^\circ$ two carbazolyl moieties take a perpendicular T-shaped orientation. Within the red rectangles at the top ($150^\circ \leq \phi \leq 180^\circ$ and 3 Å $\leq d_{COG} \leq$ 5 Å) and at the bottom ($0^\circ \leq \phi \leq 30^\circ$ and 3 Å $\leq d_{COG} \leq$ 5 Å) of Figure 3a)–c) the fraction of carbazolyl dimer pairs with ϕ close to 0° or 180° as well as 3 Å $\leq d_{COG} \leq$ 5 Å is shown for each host molecule. mCP

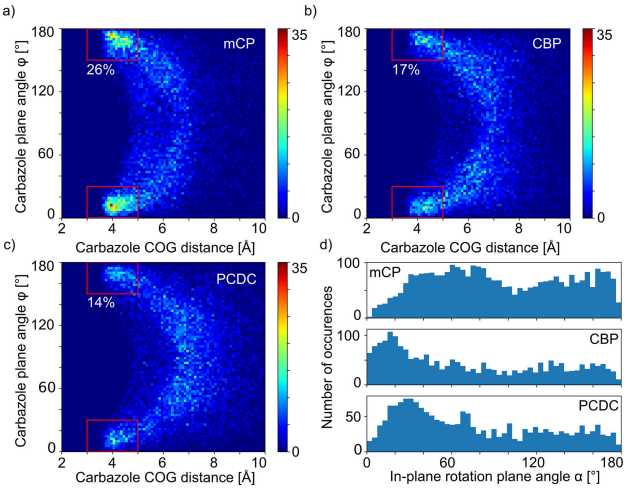

Figure 3. a) c) Heatmap plot for mCP, CBP and PCDC depicting the number of nearest neighbor carbazolyl dimer pairs as a function of the dimer stacking angle (ϕ) and the center of geometry distance (d_{COG}) between nearest neighbor terminal carbazolyl units. d) Histogram collecting the number of π stacked carbazolyl dimer pairs within the red rectangles of a) c) as a function of the relative carbazolyl in plane rotation angle α.

exhibits the largest fraction (26%) of readily formed dimers followed by CBP (17%) and PCDC (14%). An average dimer distance $d_{COG} \approx 4.0$ Å is in reasonable agreement with the computed $d_{COG}(S_0) = 3.5$ Å for both 9*H*-carbazole dimers in their electronic ground states, optimized at the MP2/def2-SV(P) level of theory (see ESI).

On closer inspection, the majority of mCP carbazolyl nearest neighbor pairs is found within $0^\circ \leq \phi \leq 60^\circ$ and $120^\circ \leq \phi \leq 180^\circ$ at distances $d_{COG} \leq 7$ Å. The picture changes for CBP, comprising most of its carbazolyl pairs within $0^\circ \leq \phi \leq 70^\circ$ and $120^\circ \leq \phi \leq 180^\circ$ at distances $td_{COG} \leq 7.5$ Å. The effect is even more pronounced for PCDC, for which a large fraction of carbazolyl pairs exhibits a stacking angle $40^\circ \leq \phi \leq 160^\circ$ at distances 6 Å $\leq d_{COG} \leq 8$ Å). Thus, the fraction of readily formed dimer pairs at small d_{COG} decreases going from mCP over CBP to PCDC, and the average d_{COG} between nearest-neighbor carbazolyl pairs increases concomitantly.

As a consequence, terminal PCDC carbazolyl groups not only have to overcome the largest distance to form molecular aggregates with their nearest neighbor, but they also have to adopt the right dimer stacking angle ϕ. Therefore, it requires the largest structural changes to form additional terminal carbazolyl aggregates in PCDC during device operation. In Figure 3d) the number of π-stacked carbazolyl dimers within the red rectangles of Figure 3a)–c) is given by a histogram, counting the occurence of specific relative carbazolyl in-plane rotation angles α. Thus, for $\phi = 0^\circ$ or $\phi = 180^\circ$, a carbazolyl in-plane angle $\alpha = 0^\circ$ corresponds to a C_{2v} dimer, whereas $\alpha = 180^\circ$ corresponds to a C_{2h} configuration. Consequently, for mCP, an antiparallel orientation (C_{2h}) is preferred, while for CBP and PCDC parallel dimers (C_{2v}) are more likely. Although the majority of the detected carbazolyl aggregates deviates from an ideal C_{2v} or C_{2h} configuration, it is expected, that (i) even these partially overlapping dimers result in a bathochromic shift of the luminescence[16,17] and/or (ii) these pre-arranged dimers form properly aligned dimers during device operation. The observed material-specific propensity to form molecular aggregates during deposition already elucidates earlier experimental observations, which indicate a particular long-term stability for PCDC in comparison to CBP and mCP.[18]

To identify the molecular mechanism, triggering EPIA during device operation by formation of additional carbazolyl aggregates, mCP, CBP and PCDC positive polarons were studied quantum chemically. Generally, EPIA is most pronounced in the presence of host positive polarons and an initial excitation energy transfer (EET) from host exciton tohost positive polaron to yield electronically excited positive polarons was suggested.[9] For EET to be efficient, a spectral overlap between the donor emission and the acceptor absorption is required. Assuming, host excitons of wide band-gap host materials to exhibit an excitation energy of ≥ 3.3 eV,[6,9,13] the radical cationic UV/VIS absorption spectra of several chosen mCP, CBP and PCDC conformers have been studied at the TDDFT/cam-B3LYP/def2-SV(P) level of theory to characterize potential electronically excited positive polaron acceptor states (for more details see Figures S1–S3) of the ESI).

While the spectra of positive polarons of mCP and PCDC exhibit a spectral area with vanishingly small absorption intensities between ~2.6 eV and ~3.6 eV and between ~2.8 eV and ~3.6 eV, respectively, no similar spectral region can be found for CBP positive polarons. Only between ~2.8 eV and ~3.1 eV the CBP radical cation UV/VIS spectrum does not show significant oscillator strengths. Yet, both mCP and CBP were found to undergo EPIA in recent experiments.[9] Unfortunately, no such experiments are available for PCDC. Based on the experimental results in combination with our calculations, the existence of a so-called *transparent window* in the positive polaron UV/VIS absorption spectrum does not necessarily eliminate EPIA.

On the other hand, we found a common acceptor state, which is available in all three *bis*-carbazolyl host materials at an energy of ~3.6 eV (see Figures S1-S3 of the ESI). This particular state resides on the terminal carbazolyl units of mCP, CBP and PCDC and corresponds to the local 9*H*-carbazole radical cation doublet state 2^2A_1. This is the only excited state with substantial oscillator strength in the deep-blue energy region (~3.6 eV) of the positive polaron UV/VIS absorption spectra of mCP and PCDC, and is also present in CBP among other suitable acceptor states. An in-depth study of the excited states dynamic of this specific 9*H*-carbazole-related excited doublet state is hardly feasible due to the relatively large molecular size of mCP, CBP and PCDC. Therefore, the 9-phenyl-9*H*-carbazole radical cation is used as model to study excited doublet state relaxation effects in *bis*-carbazolyl type positive polarons.

Calculations at the ΔSCF/B3LYP/def2-SV(P) level of theory reveal large changes in the dihedral angle γ, describing the relative orientation between the carbazolyl and the adjacent phenyl group (see Figure S4 and Table S2 of the ESI). While in the cationic ground state $\gamma \approx 130^\circ$, in the relevant excited state $\gamma \approx 90^\circ$ leading to a decoupling of the two neighboring π-systems.

In the ground state the charge is distributed over the phenyl and carbazolyl group. Vertical excitation energies of the lowest eight excited doublet states of the 9-phenyl-9*H*-carbazole radical cation were calculated using TDDFT/cam-B3LYP/def2-SV(P) along a potential energy surface (PES) scan of the dihedral angle γ in the ground state (see Figure S5). The resulting excited state PES (see Figure S6) indicate a close energetic proximity of the involved electronically excited states. These results suggest the existence of efficient non-radiative decay channels, transforming the excess electronic energy of the excited positive polaron into thermal energy. Thus, the organic host matrix is heated up locally.

The complete EPIA-based aggregation process is depicted in Figure 4. Initially, a host exciton $\left(H_D^*\right)$ is transferred onto a host positive polaron $\left(H_A^+\right)$. Subsequently, the electronically excited positive polaron $\left(H_A^{+*}\right)$ decays non-radiatively. Hence, the excess electronic energy is converted into thermal energy, which is dissipated into the local environment, which is referred to as xtitlocal heating. The released heat triggers local morphological changes, i.e. vibrational motion, which eventually yield molecular aggregation between the terminal carbazolyl units of neighboring host molecules. The resulting

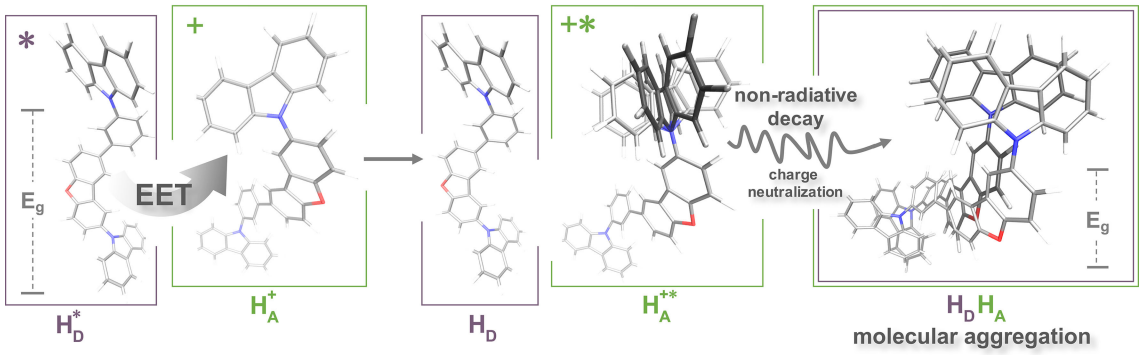

Figure 4. At the example of PCDC, the mechanistic features of EPIA are illustrated. Upon EET from host exciton (H_D^*) to host positive polaron (H_A^+), the electronically excited positive polaron (H_A^{+*}) decays non radiatively. Hence, the excess electronic energy is efficiently converted into thermal energy, which is dissipated into the local environment. The released heat triggers local morphological changes, which eventually yield molecular aggregation between the terminal carbazolyl units of neighboring host molecules. The resulting aggregates exhibit a smaller band gap E_g and a lower phosphorescence emission energy than the corresponding monomer species, which explains experimentally observed bathochromic shifts in the corresponding luminescence spectra.

aggregates exhibit a smaller band-gap E_g and a lower phosphorescence emission energy ($\Delta E(T_1)@T_1$) than the corresponding monomer species, which is one very likely mechanism for the experimentally observed red-shift in the luminescence spectra of degraded devices.[9,12]

Although the suggested local heating mechanism affects all three host materials, our results strongly imply the impact of EPIA to depend on the molecular structure. Thus, limited propensity to readily form molecular aggregates in combination with suitable photophysical characteristics, i.e. a transparent window, determining the number of successful exciton to positive polaron EET processes, are required material-specific conditions for a long-term stable blue PhOLED host material.

Along this line of thought, mCP exhibits the highest tendency to form carbazolyl aggregates with a particularly small mean distance between neighboring terminal carbazolyl units (Figure 3a). Therefore, despite its pronounced transparent window (Figure S1), mCP is clearly affected by molecular aggregation as its morphology is prone to form carbazolyl dimers in response to local heating. On the other hand, CBP, which has a low tendency to form aggregates, exhibits a significant number of potential acceptor states in its cationic absorption spectrum. Thus, the structural advantages of CBP are overcompensated by numerous EET processes during device operation, which eventually trigger EPIA. Finally, PCDC exhibits the most disordered host matrix with relatively large nearest-neighbor carbazolyl distances, as well as a large transparent window in the positive polaron absorption spectrum. PCDC thus fulfills both conditions, which are assumed to prolong the device lifetime as EPIA is efficiently avoided. In particular, the unsymmetric bridge, connecting the terminal carbazolyl units of PCDC, helps to lower the overall carbazole concentration in the matrix and increases the disorder, while each of the underlying 9-phenyl-9*H*-carbazole, 9*H*-carbazole and dibenzo[*b,d*]furan molecular fragments comprises a transparent window in its radical cationic absorption spectrum.[19]

It is beyond the scope of this work to address differences between red, green and blue PhOLED in great detail, yet, local heating most likely also applies for longer-lived green and red PhOLEDs. While the host exciton energy increases going from red to blue, the energetic position of the positive polaron's lowest excited doublet state remains approximately the same (for details see the ESI). Thus, the amount of excess energy, converted into heat during the non-radiative relaxation of the positive polaron, significantly increases going from red to green and blue PhOLEDs leading to stronger local heating.

3. Conclusions

Compared to existing literature, our results explain the recent experimental findings on the degradation of *bis*-carbazolyl host materials used in (blue) PhOLEDs.[12] There, two types of morphological changes were investigated: (i) longer-range ordering (crystallization) caused by thermal stress and (ii) short-range molecularpairing (e.g. dimerization or trimerization).[12] Indeed, under thermal stress long-range crystallization of the device is observed, while under device operation only local morphological changes are found.

The latter observation perfectly agrees with local heating, which is explained by our suggested mechanism of decaying excited host positive polarons. Local heating leads to carbazolyl type aggregates and the propensity to their formation is a material-specific parameter. Therefore, the choice of a suitable molecular core, connecting the terminal carbazolyl moieties, is of utmost importance and will be the subject of future investigations. The presented findings provide an explanation for EPIA-based degradation in wide band-gap hosts and deliver new impulses to systematically tune high-performance materials.

Computational Details

9*H*-carbazole dimer initial guess structures were prepared in C_{2v} and C_{2h} symmetry, respectively, while the 9*H*-carbazole monomer coor-

dinates were prepared in C_{2v} symmetry. Ground- and excited state optimizations for singlet and triplet states were carried out within the TURBOMOLE 7.0 program package[20,21] at the RI-MP2[22 25] and RI-ADC(2)[22,23,26 32] level of theory using the resolution-of-the-identity (RI) approximation together with the def2-SV(P) basis set and the corresponding auxiliary basis functions.[33 35] Vertical excitation energies were obtained at the RI-ADC(2)/def2-SV(P) level (compare Figure 2 and Table S1). For both the excited state calculations and the geometry optimizations the frozen core approximation was invoked.

The amorphous host-only morphologies, that have been employed for statistical analyses, were calculated using the Metropolis Monte Carlo based simulated annealing method.[36] This vapor deposition simulation consists of 10 simulated annealing cycles per molecule with 150000 Metropolis Monte Carlo steps per cycle. In each cycle, the temperature is decreased from 4000 K to 300 K, while the molecule can explore the potential energy surface of the already deposited and frozen film. The energy of the new molecules is evaluated using a classical force-field consisting of electrostatic interaction between DFT-derived partial charges, a standardized 12-6-potential to model the Lennard-Jones interaction as well as a molecule specific dihedral force-field to evaluate internal degrees of freedom. The dihedral force-field was derived using semi-empirical PM6 calculations. Apart from dihedral rotations, all other internal degrees of freedom are kept frozen. The parent molecular structure used in the deposit procedure outlined above was initially optimized at the B3LYP/def2-SV(P) level of theory using the TURBOMOLE 7.0 program package.[20,21,34,37 43] For each of the host materials studied in this work (mCP, CBP and PCDC) 5 independent morphologies were generated, each including 1500 molecules.

In order to avoid artifacts, the molecules in the lowest 10 Angstroms were discarded of the final morphologies. The remaining molecules were used to analyze the relative orientations of carbazole units of neighboring molecules (compare Figure 3).

UV/VIS absorption spectra of the mCP, CBP and PCDC positive polarons (radical cations) were simulated at the TDDFT/cam-B3LYP/def2-SV(P)[34,43 46] levelof theory (compare Figures S1 S3) within the Q-Chem 4.4 program package.[47] To account for conformational effects on the spectral shape, molecular structures of mCP, CBP and PCDC conformers were taken from the simulated amorphous morphologies. TDDFT/cam-B3LYP/def2-SV(P) has been chosen based on a thorough method benchmarking (involving several approximate density functionals and IP-ADC(2)), that wasconducted for the aforementioned conformers of the mCP, CBP and PCDC radical cations. Here, the TDDFT/cam-B3LYP/def2-SV(P) results were in good agreement with IP-ADC(2)/def2-SV(P) and thus in the present work TDDFT/cam-B3LYP/def2-SV(P) was employed to study relative trends in the UV/VIS absorption spectra of the mCP, CBP and PCDC radical cations. For a compact representation of excited state characters, electron-/hole-densites[48,49] (e/h densities), shown in Figures S1 S3, were computed. In the combined e/h-plots the hole density (red) is that part of the electron density, which is taken away upon excitation and rearranged aselectron-density (blue). In case of an open-shell wavefunction two sets of e/h-densities occur, namely e/h-densities for the α and the β spin electrons. In Figures S1 S3, only the e/h-β-densities are shown since e/h-α-densities are approximately zero for the excited states under consideration.

For the 9-phenyl-9*H*-carbazole model system ground and excited state geometries were optimized without symmetry using the ΔSCF approach at the B3LYP/def2-SV(P)[37 42] level of theory within the Q-Chem 4.4 program package, where B3LYP was invoked using VWN(V) (Figure S4).[39] In order to converge the ΔSCF procedure to the desired excited electronic configuration the maximum overlap method (MOM)[50] was employed. Dihedral angle scans for the 9-phenyl-9*H*-carbazole cation have been conducted at the RI-BP86/def2-TZVP[33,34,37 40,51 53] and the cam-B3LYP/def2-SV(P)[34,43,46] level of theory (Figure S5). While the cam-B3LYP/def2-SV(P) results were obtained using the Q-Chem 4.4 program package,[47] the RI-BP86/def2-TZVP geometry optimizations were conducted using the TURBOMOLE 7.0 package.[20,21]

RMSD values were calculated within the JMol visualization package.[54] Based on the RI-BP86/def2-TZVP optimized ground state structures, the relative energetic order of the lowest eight excited doublet states of the 9-phenyl-9*H*-carbazole cation, was computed at the TDDFT/cam-B3LYP/def2-SV(P) level of theory within the Q-Chem 4.4 program package (Figure S6).

Supplementary Information

Supplementary information is available containing: 9*H*-carbazole monomer/dimer excitation energies, simulated positive polaron absorption spectra of mCP, CBP and PCDC, ΔSCF results and PES simulations for 9-phenyl-9*H*-carbazole cation model (PDF).

Acknowledgement

The morphology simulations were performed on the computational resource ForHLR I funded by the Ministry of Science, Research and the Arts Baden-Württemberg and DFG ("Deutsche Forschungsgemeinschaft"). The authors thank BASF SE for continuous support.

Conflict of Interest

The authors declare no conflict of interest.

Keywords: aggregation quenching · degradation · organic electronics · phosphorescence · quantum chemistry

[1] Mark Rogowsky Thanks To Apple, Top Rival Samsung Keeps Winning. accessed: 2017 09 08.
[2] S. R. Forrest, M. A. Baldo, D. F. O'Brien, Y. You, A. Shoustikov, S. Sibley, M. E. Thompson, *Nature* **1998**, *395*, 151 154.
[3] C. Adachi, M. A. Baldo, M. E. Thompson, S. R. Forrest, *J. Appl. Phys.* **2001**, *90*, 5048 5051.
[4] H. Yersin, *Highly Efficient OLEDs with Phosphorescent Materials*. Wiley VCH Verlag GmbH & Co. KGaA, Weinheim, **2008**.
[5] J. F. Tremblay, *Chem. Eng. News* **2016**, *94*, 30 34.
[6] J. Lee, C. Jeong, T. Batagoda, C. Coburn, M. E. Thompson, S. R. Forrest, *Nat. Commun.* **2017**, *8*, 15566.
[7] S. Scholz, D. Kondakov, B. Lüssem, K. Leo, *Chem. Rev.* **2015**, *115*, 8449 8503.
[8] S. Schmidbauer, A. Hohenleutner, B. König, *Adv. Mater.* **2013**, *25*, 2114 2129.
[9] Q. Wang, B. Sun, H. Aziz, *Adv. Funct. Mater.* **2014**, *24*, 2975 2985.
[10] Q. Wang, H. Aziz, *Adv. Opt. Mater.* **2015**, *3*, 967 975.
[11] Y. Zhang, H. Aziz, *ACS Appl. Mater. Interfaces* **2016**, *8*, 14088 14095.
[12] H. Yu, Y. Zhang, Y. J. Cho, H. Aziz, *ACS Appl. Mater. Interfaces* **2017**, *9*, 14145 14152.
[13] S. T. Hoffmann, P. Schrögel, M. Rothmann, R. Q. Albuquerque, P. Strohriegl, A. Köhler, *J. Phys. Chem. B* **2011**, *115*, 414 421.

[14] G. E. Johnson, *J. Phys. Chem.* **1974**, *78*, 1512 1521.
[15] R. W. Bigelow, G. E. Johnson, *J. Chem. Phys.* **1977**, *66*, 4861 4871.
[16] K. Tani, Y. Tohda, H. Takemura, H. Ohkita, S. Ito, M. Yamamoto, *Chem. Commun.* **2001**, *50*, 1914 1915.
[17] P. de Sainte Claire, *J. Phys. Chem. B* **2006**, *110*, 7334 7343.
[18] Christian Lennartz, BASF SE, private communication.
[19] T. Shida, *Electronic Absorption Spectra of Radical Ions (Physical Sciences Data).* Elsevier Science Ltd, **1989**.
[20] R. Ahlrichs, M. Bär, M. Häser, H. Horn, C. Kölmel, *Chem. Phys. Lett.* **1989**, *162*, 165 169.
[21] TURBOMOLE GmbH TURBOMOLE V7.0 2015, a development of University of Karlsruhe, Forschungszentrum Karlsruhe GmbH, 1989 2007, TURBOMOLE GmbH, since 2007; available from http://www.turbomole.com.
[22] C. Hättig, F. Weigend, *J. Chem. Phys.* **2000**, *113*, 5154.
[23] C. Hättig, A. Hellweg, A. Köhn, *Phys. Chem. Chem. Phys.* **2006**, *8*, 1159, 2006.
[24] F. Weigend, M. Häser, *Theor. Chem. Acc.* **1997**, *97*, 331 340.
[25] C. Hättig, *J. Chem. Phys.* **2003**, *118*, 7751 7761.
[26] J. Schirmer, *Phys. Rev. A* **1982**, *26*, 2395 2416.
[27] A. B. Trofimov, J. Schirmer, *J. Phys. B: At. Mol. Opt. Phys.* **1995**, *28*, 2299 2324.
[28] C. Hättig, A. Köhn, *J. Chem. Phys.* **2002**, *117*, 6939 6951.
[29] C. Hättig, K. Hald, *Phys. Chem. Chem. Phys.* **2002**, *4*, 2111 2118.
[30] C. Hättig, A. Köhn, K. Hald, *J. Chem. Phys.* **2002**, *116*, 5401 5410.
[31] A. Köhn, C. Hättig, *J. Chem. Phys.* **2003**, *119*, 5021 5036.
[32] C. Hättig, *Adv. Quantum Chem.* **2005**, *50*, 37 60.
[33] F. Weigend, M. Häser, H. Patzelt, R. Ahlrichs, *Chem. Phys. Lett.* **1998**, *294*, 143 152.
[34] F. Weigend, R. Ahlrichs, *Phys. Chem. Chem. Phys.* **2005**, *7*, 3297.
[35] C. Hättig, *Phys. Chem. Chem. Phys.* **2005**, *7*, 59 66.
[36] T. Neumann, D. Danilov, C. Lennartz, W. Wenzel, *J. Comp. Chem.* **2013**, *34*, 2716 2725.
[37] P. A. M. Dirac, *Proc. R. Soc. A: Math. Phys. Eng. Sci.* **1929**, *123*, 714 733
[38] J. C. Slater, *Phys. Rev.* **1951**, *81*, 385 390
[39] S. H. Vosko, L. Wilk, M. Nusair, *Can. J. Phys.* **1980**, *58*, 1200 1211.
[40] A. D. Becke, *Phys. Rev. A* **1988**, *38*, 3098 3100.
[41] C. Lee, W. Yang, R. G. Parr, *Phys. Rev. B* **1988**, *37*, 785 789.
[42] A. D. Becke, *J. Chem. Phys.* **1993**, *98*, 5648 5652.
[43] A. Schäfer, H. Horn, R. Ahlrichs, *J. Chem. Phys.* **1992**, *97*, 2571 2577.
[44] E. Runge, E. K. U. Gross, *Phys. Rev. Lett.* **1984**, *52*, 997 1000.
[45] M. E. Casida Time Dependent Density Functional Response Theory for Molecules. In *Recent Advances in Density Functional Methods, Part I*, pages 155 192. World Scientific, Singapore, **1995**.
[46] T. Yanai, D. P. Tew, N. C. Handy, *Chem. Phys. Lett.* **2004**, *393*, 51 57.
[47] Y. Shao, *Mol. Phys.* **2015**, *113*, 184 215.
[48] F. Plasser, M. Wormit, A. Dreuw, *J. Chem. Phys.* **2014**, *141*, 024106.
[49] F. Plasser, A. Dreuw, *J. Phys. Chem. A* **2015**, *119*, 1023 1036.
[50] A. T. B. Gilbert, N. A. Besley, P. M. W. Gill, *J. Phys. Chem. A* **2008**, *112*, 13164 13171.
[51] J. P. Perdew, *Phys. Rev. B* **1986**, *33*, 8822 8824.
[52] K. Eichkorn, F. Weigend, O. Treutler, R. Ahlrichs, *Theor. Chem. Acc.* **1997**, *97*, 119 124.
[53] F. Weigend, *Phys. Chem. Chem. Phys.* **2006**, *8*, 1057.
[54] Jmol. Jmol: an open source Java viewer for chemical structures in 3D. http://www.jmol.org/.